TRI-PP-76-3
July 1976

Production of Low-Energy Charged Pions by 580 MeV Protons on Various Nuclei*

P.W. Jacobs, D.V. Bryman,‡ G.R. Mason, L.P. Robertson, T.R. Witten††
TRIUMF and Dept. of Physics, University of Victoria, Victoria, B.C., Canada V8W 2Y2

J.S. Vincent‡
NASA, Lewis Research Center, Cleveland, Ohio

Abstract

The production cross sections for positive and negative pions by 580 MeV protons on Be, C, Cu, and Pb have been measured for pion energies from 20 to 100 MeV and production angles from 60° to 150°. The differential cross sections for pion energies below 50 MeV are nearly isotropic for angles between 60° and 150°, while at higher energies the cross sections are predominantly forward peaked.

(submitted to Phys. Rev. C)

*Research supported by the Atomic Energy Control Board of Canada
†Now at AECL, Chalk River Nuclear Laboratories, Chalk River, Ontario
‡Now at TRIUMF, Vancouver, B.C., Canada V6T 1W5
††Now at Kent State University, Kent, Ohio 44242

I. INTRODUCTION

Pion production cross sections for nucleons on nuclei provide basic data for the study of pion physics and nuclear structure. Such data are also important for the design of pion beam channels.

An extensive set of measurements for 730 MeV protons has been reported by Cochran *et al.*[1] for various targets at several angles from 15° to 150°, and pion energies from 25 to 550 MeV. At 600 MeV Hirt *et al.*[2] have measured cross sections at 0.8° and 21.5° for several pion energies from 50 to 350 MeV. Pion production by protons has also been measured at 660 MeV by Meshkovskii *et al.*,[3] at 625 MeV by Haddock *et al.*,[4] and at 450 MeV by Lillethun.[5] A more complete list of references to pion production by intermediate energy protons is given in reference 1.

Theoretical attempts[6-9] to fit existing data indicate the need for additional measurements of the differential cross sections for producing low energy pions at large angles.

The work described here was undertaken in order to augment the existing data on production of pions by protons with energy near 600 MeV. Production cross sections have been measured for both positive and negative pions at five angles from 60° to 150°, and for five energies between 20 and 100 MeV for 580 MeV proton bombardment of targets of Be, C, Cu and Pb. Measurements of the positive pion production cross sections for carbon were made at 22° for comparison with the measurements of Hirt *et al.*[2]

II. EXPERIMENTAL TECHNIQUE

The experiment was performed using the 580 MeV external proton beam from the synchrocyclotron at the Space Radiation Effects Laboratory (SREL).* Both positive and negative pions were detected using two similar pion range telescopes each consisting of five scintillation counters made of NE102† (see Fig. 1). The energies of the pions stopping in counter 4 of each telescope were selected by varying the amount of copper degrader placed between counters 2 and 3. By measuring the time-of-flight between counters 1 and 2, and the pulse-heights in counter 3 and in counter 4, for each stopping particle, it was possible to distinguish pions and muons from protons and electrons. Thin polyethylene bags containing helium gas were placed between the target and counter 1, and between counters 1 and 2, in order to reduce multiple scattering. The dimensions of the counters in the two telescopes are listed in Table I. For each position and pion energy of the range telescopes, the measurements were made sequentially for four targets and a no-target background.

Positive pions were identified by observing the muon from the pion decay, $\pi^+ \rightarrow \mu^+ + \nu$. The signal for a positive pion consisted of a five-fold coincidence, $1.2.3.4.\overline{5}$, indicating a particle stopping in counter 4 and a subsequent three-fold coincidence, $3.4.\overline{5}$, indicating

† Nuclear Enterprises Ltd., 935 Terminal Way, San Carlos, California, U.S.A. 94070.

* SREL is supported by the National Science Foundation, the State of Virginia, and the National Aeronautics and Space Administration.

the decay muon detected in counter 4. Thus an "event" signal was generated when a second pulse occurred in counter 4 during a 100 nsec gate beginning 23 nsec after a stop signal. The anti-coincidence requirements on counters 3 and 5 ensured that this second pulse was not caused by another particle traversing the telescope following the stop signal.

Negative pions need to be identified by a different technique because fewer than 0.01% decay after stopping in counter 4. The detection of a negative "pion star" was required in counter 4 as the π^- event signature.[10] The term "pion star" refers to the large amount of energy released when a pion is captured by a nucleus. The discriminator level on counter 4 was set low enough to detect a significant fraction of the π^- stars but high enough to have a small efficiency for detecting stopped muons. Measurements of the relative efficiencies made in pion and muon beams are discussed in section B. Thus the negative pion signature was $1.2.3.4_s.\overline{5}$, where the s implies a relatively high threshold on counter 4. To reduce the flux of protons which also produced large pulses in the stopping counter 4, a 45° bending magnet was included in the π^- telescope system as shown in Fig. 1. The magnet was set for negative particles with central momentum corresponding to the pions stopping in the telescope. This enabled the star detector to be used for π^- identification in the presence of the large proton flux coming from the target.

An "on-line" data acquisition system[11] using the SREL IBM 360/44 computer was used to record for each event in each telescope the time-of-flight between counters 1 and 2 and the pulse amplitudes in counters 3 and 4, as well as to record scaled data such as the beam intensity monitor. The data acquisition program generated histograms of the various telescope parameters permitting the monitoring of the detection systems during the runs. A preliminary cross section value was calculated by the program on the completion of each run. The three parameters recorded for each event permitted "off-line" analysis to be used to give good separation of the π events from events due to protons and electrons.

A. Beam Monitoring

The proton beam intensity was monitored using a "scattered-beam" telescope made up of three scintillation counters to detect particles scattered from an aluminum target placed in the beam several meters beyond the pion production target. This monitor was calibrated absolutely using two methods. In the first method the monitor was calibrated in terms of the measured cross section for the production of ^{11}C by the $^{12}C(p,pn)^{11}C$ reaction (30.8 ± 1.5 mb).[12] For this case a carbon foil was activated in the beam and the subsequent β^+ activity from the ^{11}C measured relative to that from a calibrated ^{22}Na source by counting the annihilation radiation with a NaI(Tℓ) scintillation detector. In the second method, a "beam intercepting" scintillation counter telescope was placed directly in the proton beam. At a reduced intensity of approximately 10^5 protons/sec, the fraction of "scattered-beam" monitor telescope events in coincidence with the beam intercepting telescope events was measured, giving the efficiency of the "scattered-beam" telescope directly. The results obtained by the two methods are given in Table II and are in good agreement.

B. Data Analysis

The cross sections were calculated using the equation:

$$\frac{d^2\sigma}{d\Omega\, dT_\pi} = \frac{N_\pi}{N_p\, \rho_t\, \Omega\, \Delta T_\pi\, \epsilon_\pi\, \epsilon_d\, \epsilon_a\, \epsilon_s\, \epsilon_m} ,$$

where N_π is the number of pion events detected; N_p is the number of protons incident on the target as determined from the number of monitor counts recorded and the monitor calibration; ρ_t is the number of target atoms per unit area normal to the beam; Ω is the geometrical solid angle; ΔT_π is the energy acceptance of the pion telescope determined from range and energy-loss tables[13]; ϵ_π is the pion detection factor, defined as the ratio of pions detected to pions stopped in counter 4; ϵ_d is the non-decay probability for a pion between the production target and counter 4; ϵ_a is the probability the pion will not be lost because of nuclear absorption or inelastic scattering; ϵ_s is the probability that a pion will not be lost because of nuclear elastic scattering; ϵ_m is the probability that a pion will not be lost because of multiple Coulomb scattering, calculated using a Monte Carlo method.[14]

Details of the evaluation of Ω, ε_π, ε_a, ε_s and ε_m are discussed below. Values of the various parameters for the positive pion telescope are given for the five pion energies in Table III.

The solid angle, Ω, of the π^+ telescope defined by counter 2 was calculated to be 1.17 ± 0.01 msr using a Monte Carlo program.[14] The solid angle for the π^- telescope was calculated for each production angle and pion energy using a ray tracing program to track pions through the measured magnetic field of the bending magnet. This included the effects of the vertical focussing of the rectangular magnet and the dispersion across the solid angle defining counter 2; the solid angle for the π^- telescope was a function of the production angle.

The positive pion detection factors, ε_{π^+}, for the telescopes were measured using pion beams from meson channels at SREL[15] and at the 184" cyclotron at the Lawrence Berkeley Laboratory.[16] ε_{π^+} was found to be 0.390 ± 0.008 for the π^+ telescope and 0.38 ± 0.01 for the π^- telescope. The latter measurement enabled the same π^+ cross sections to be measured in both telescopes for a consistency check. The measured ε_{π^+} is in agreement with the value calculated for the probability that a positive pion will decay during a 100 ± 5 nsec period 23 ± 1 nsec after stopping in counter 4 using the measured value of the π^+ lifetime.[17] Positive muons stopping in counter 4 may also give an "event" signal from the positron pulse produced in the decay $\mu^+ \rightarrow e^+ + \nu + \bar{\nu}$; however, because of the longer lifetime

of the muon and the greater range of the positron, the relative muon detection factor is less than 1% that of pions.

The negative pion and muon star detection factors, ε_{π^-} and ε_{μ^-}, were also measured for the π^- telescope using the SREL meson channel. The results of these measurements are shown in Fig. 2 where the measured detection factor is plotted as a function of the discriminator level on the counter 4 pulse height. During the experiment the discriminator level was set typically so that the π^- detection factor was 0.18, and so the μ^- detection factor was less than 0.2% of that for π^-. Thus no correction for muon contamination in the event spectra was necessary.

ε_a, the probability that a pion will not be lost because of nuclear absorption or inelastic scattering in the material in front of counter 4, was calculated for each pion energy by using empirical fits to measured values of the total nonelastic cross sections for pions in carbon and copper.[18-23] The curves used are shown in Fig. 3. The absorption occurs predominantly in the copper degrader and is the limitation for extending this method for detecting pions to energies much above 100 MeV.

The much smaller correction for the probability that a pion will not be elastically scattered in the material in front of counter 4 and miss this counter, ε_s, was calculated assuming the ratio of elastic to non-elastic cross sections was 0.6 [22,24,25] and that 20% of

those pions which elastically scattered would miss counter 4 based on published angular distribution measurements.[22,23,24,26,27] This correction is only significant for the 100 MeV measurements and even here uncertainties due to the assumption produce a negligible contribution to the uncertainty in the cross sections. The contribution from pions of higher energy being inelastically scattered in the material in front of counter 4 and stopping in counter 4 was estimated to be less than 0.1% in the worst case.

C. Accuracy of the Measurements

Uncertainties in the cross sections were calculated by adding in quadrature the rms errors of the individual parameters entering into the cross section formula; typical values contributed by the various factors are given in Table IV. The statistical uncertainties in N_π include those arising from background corrections and from uncertainties in setting the time-of-flight and pulse-height limits. They are typically ± 3% for the π^+ data and up to ± 15% for the lower yield π^- data at 100 MeV pion energy.

Uncertainties in the parameters N_p and ε_π contribute to the uncertainty in the absolute normalization of the data. Error in N_p is due to the uncertainty in the monitor calibration. Recently a check has been made of the π^+ telescope efficiency by measuring the yield of positive pions from the reaction $p + p \rightarrow \pi^+ + d$ at proton energies between 400 and 500 MeV. The results agree with the published values for this cross section and confirm the telescope efficiency.[28]

III. EXPERIMENTAL RESULTS

The values measured for the differential production cross sections, $d^2\sigma/dT_\pi d\Omega$, for positive and negative pions are given in Tables V to VIII for targets of Be, C, Cu and Pb. The errors listed in these tables include only the relative errors; there is a common normalization error of ± 6% for π^+ and ± 11% for π^- not included.

The total cross sections σ_T^+ and σ_T^- were calculated from the differential cross sections reported here and from the 0.8° and 21.5° data measured by Hirt *et al.*[2] by integrating over pion energy and production angle. The results of these calculations and the ratios of π^+ to π^- production cross sections are given in Table IX. Approximately 35% of the total cross section came from measurements of Hirt *et al.* The results for the four targets for the π^+ total cross sections are given to a good approximation by $\sigma_T^+ = 11.2\ Z^{1/3}$ mb as a function of atomic number Z, and similarly for the π^- total cross sections by $\sigma_T^- = 1.0\ N^{2/3}$ mb as a function of neutron number N. These results can be compared with similar fits by Cochran *et al.*[1] to their 730 MeV production data for which they found $\sigma_T^+ = 24.5\ Z^{1/3}$ and $\sigma_T^- = 2.33\ N^{2/3}$. Thus the total cross sections at 730 MeV are approximately a factor two larger for both π^+ and π^- yields compared to the results at 580 MeV reported here.

The π^+ differential production cross sections measured for carbon at 22° can be compared to similar measurements by Hirt *et al.*[2] These data are shown in Fig. 4. The results from the two measurements for

100 MeV π^+ are within the statistical errors on the data, the result reported here being 20% lower than that of Hirt. The result for 50 MeV π^+ reported here is nearly a factor two lower than that of Hirt *et al.*[2] Comparison of π^- differential cross sections at 22° was not possible because of limitation on the angular range accessible to the π^- telescope. Measurements of the π^+ cross sections at 90° from Cu and Pb were made using the π^- telescope and the results agreed with the values measured with the π^+ telescope within the experimental accuracy.

IV. CONCLUSIONS

The results of positive and negative pion production cross section measurements from 580 MeV protons at low energies show that the low energy π^+ cross sections are largest in the angular range 120° to 135°, while the production of low energy π^- cross sections are nearly isctropic for angles between 60° and 135°. For 580 MeV protons at backward angles the production cross sections show a maximum in the pion energy range between 30 and 40 MeV.

In Figs. 5 and 6 a comparison is shown between the results reported here and those reported by Cochran *et al.*[1] measured for 730 MeV protons; the differential production cross sections for positive and negative pions from carbon are plotted as a function of pion energy for laboratory angles of 60, 90, 120, 135 and 150°. At both bombarding energies, the low energy pions are produced almost isotropically, while high energy pions are produced predominantly in

the forward direction. At the backward angles, with increasing proton energy, the peak moves to higher pion energies. However, the differential cross sections for low energy pions does not change much with increasing proton energy and in many cases it is higher at 580 MeV than at 730 MeV. Increasing proton energy increases the yield of higher energy pions.

The π^+ differential cross sections at about 20° from carbon measured for various proton energies are plotted in Fig. 4. The results reported here measured at 580 MeV are shown as well as the results of Hirt *et al.*[2] at 595 MeV, and those of Cochran *et al.*[1] at 730 MeV, Meshkovskii *et al.*[3] at 660 MeV, and Lillethun[5] at 450 MeV. The cross sections measured by Lillethun[5] disagree markedly with the trend indicated by other results, and with recent measurement at 450 MeV.[28]

Beder and Bendix[6] have calculated the double differential cross sections for π^+ production from carbon by 580 MeV protons using a semi-classical model for pion production. The production rate is given in terms of the momentum averaged free production rate multiplied by an absorptive attenuation factor; the free production matrix element is normalized to the measured pp → pn π^+ cross sections. They fit the 0° and 21.8° π^+ carbon data of Hirt *et al.*[2]; their 22° curve is shown in Fig. 7 along with the measured data of Hirt *et al.*[2] and the results reported here. Using the same parameters, they have also calculated[7] the differential π^+ cross sections from carbon and copper for 580 MeV protons at the larger angles investigated here. These comparisons

are also given in Fig. 7. The error flags in the experimental data points do not include the 6% normalization uncertainty. The accuracy of the theoretical calculation is estimated to be about ± 10%. The agreement with the experimental data at forward and backward angles is good, whereas at angles of 60° and 90° the calculation appears to predict too many high energy pions.

The results of the measurements reported here and those measured at 730 MeV provide important information for the design of pion beam channels for intermediate energy proton accelerator facilities. Low energy pion production is almost isotropic; in fact, the cross sections increase slightly between 120° and 135°. Therefore it is advantageous to locate a pion channel at backward angles from the production target where the lower neutron and proton yields can be used to improve the pion to background ratio. For a higher energy pion channel a production angle forward of 90° must be used.

ACKNOWLEDGEMENTS

It is a pleasure to acknowledge the support of the director, Dr. R.T. Siegel, and the staff of the Space Radiation Effects Laboratory, Newport News, Virginia, for making the facilities of the laboratory available to us. We wish to thank Dr. T.R. King for his assistance during the final data taking run. One of us, (P.W.J.), acknowledges financial assistance from the National Research Council of Canada.

REFERENCES

1. D.R.F. Cochran, P.N. Dean, P.A.M. Gram, E.A. Knapp, E.R. Martin, D.E. Nagle, R.B. Perkins, W.J. Schlaer, H.A. Thiessen and E.D. Theriot, Phys. Rev. D6 3085 (1972).

2. W. Hirt, E. Heer, M. Martin, E.G. Michaelis, C. Serre, P. Skarek and B.T. Wright, European Organization for Nuclear Research Report CERN 69-24 (1969).

3. A.G. Meshkovskii, II. Shalamov and V.A. Shevanov, Soviet Phys. JETP 34, 987 (1958).

4. R.P. Haddock, M. Zeller and K.M. Crowe, University of California at Los Angeles Report UCLA-MPG 64-2 (1964).

5. E. Lillethun, Phys. Rev. 123, 665 (1962).

6. D.S. Beder and P. Bendix, Nucl. Phys. B26, 597 (1971).

7. D.S. Beder and P. Bendix, Private Communication (1975).

8. M.M. Sternheim and R.R. Silbar, Phys. Rev. D6, 3117 (1972).

9. D.A. Sparrow, M.M. Sternheim and R.R. Silbar, Phys. Rev. C10, 2215 (1974).

10. A. Citron, C. Delorme, D. Fries, J. Heintze, E.G. Michaelis, H. Overas and Y. Shtcherbakov, Nucl. Instr. and Meth. 15 121 (1962).

11. H.L. Gelenter, J. Birnbaum, M. Mikelsons, J.D. Russell, F. Cochrane, D. Groff, J.F. Schofield and D.A. Bromley, Nucl. Instr and Meth. 54, 77 (1967)

12. J.B. Cumming, Ann. Rev. of Nucl. Sci. 13, 261 (1963).

13. W.H. Barkas and M.J. Berger, *Tables of Energy Losses and Ranges of Heavy Particles*, NASA Report SP-3013 (1964).

14. P. Kitching, TRIUMF Report TRI-71-2 (1971) and G.Stinson and P. Kitching, TRIUMF Report TRI-DNA-73-4 (1973).

15. H.O. Funsten, Nucl. Instr. and Meth. 94, 443 (1971).

16. P.A. Reeve, L.P. Robertson, N.M. AlQazzaz and C.H.Q. Ingram, Nucl. Instr. and Meth. 114 , 105 (1974).

17. V. Chaloupka, C. Bricman, A. Barbaro-Galtieri, D.M. Chew, R.L. Kelly, T.A. Lasinski, A. Rittenberg, A.H. Rosenfeld, T.G. Trippe, R. Uchiyama, N. Barash-Schmidt, P. Soding and M. Roos, Phys. Lett. 50B, 1974 (1974).

18. C. Chedester, P. Isaacs, A. Sachs and J. Steinberger, Phys. Rev. 82, 958 (1951).

19. R.L. Martin, Phys. Rev. 87, 1052 (1952).

20. D.H. Stork, Phys. Rev. 93, 868 (1954).

21. A.E. Ignatenko, A.I. Mukhin, E.B. Ozerov and B.M. Pontecorvo, Soviet Phys. JETP 4, 351 (1956).

22. V.P. Dzkelepov, V.G. Ivanov, M.S. Kozodaev, V.T. Osipenkov, N.I. Petrov and V.A. Rusakov, Soviet Phys. JETP 4, 864 (1957).

23. F. Binon, P. Duteil, J.P. Garron, J. Gorres, L. Hogon and J.P. Peigneux, Nucl. Phys. B17, 168 (1970).

24. J.O. Kessler and L.M. Lederman, Phys. Rev. 94, 689 (1954).

25. D.S. Koltun, Advances in Nuclear Physics 3, 71 (1969).

26. W.F. Baker, J. Rainwater and R.E. Williams, Phys. Rev. 112, 1763 (1958).

27. T.A. Fujii, Phys. Rev. 113, 695 (1959).

28. E.L. Mathie, G.A. Beer, G.R. Mason, A. Olin, L.P. Robertson, D.A. Bryman and J.S. Vincent. To be published.

TABLE I

TELESCOPE COMPONENT DIMENSIONS

SCINTILLATORS

Telescope	Counter No.	Height (cm)	Width (cm)	Thickness (gm/cm^2)
π^+	1	3.81	3.81	0.164
	2	8.89	8.89	0.328
	3	15.2	15.2	1.31
	4	11.4	11.4	0.655
	5	12.7	12.7	0.655
π^-	1	5.08	7.62	0.082
	2	15.2	15.2	0.328
	3	20.3	20.3	1.31
	4	17.8	17.8	1.31
	5	25.4	25.4	0.655

Cu DEGRADERS

Telescope	T_π (MeV)	Absorber Thickness (gm/cm^2)	
		between 2 and 3	between 3 and 4
π^+	21	0	0
	30	0	2.82
	52	8.63	2.82
	76	20.25	2.82
	100	33.61	2.82
π^-	22	0	0
	32	0	2.91
	53	8.64	2.91
	76	20.14	2.91
	102	34.30	2.91

TABLE II

PROTON BEAM MONITOR CALIBRATIONS[a]

(units 10^5 protons/monitor counts)

By comparison with:	#1	#2
C^{12} (p, pn) C^{11} Activation Method	1.74 ± 0.09	1.41 ± 0.07
Beam Intercepting Telescope	1.70 ± 0.02	1.36 ± 0.02
Weighted Average	1.70 ± 0.02	1.36 ± 0.02

a The difference between calibrations #1 and #2 is due to a change made in the detection solid angle of the proton beam monitor.

TABLE III

Calculated Parameters for the Positive Pion Telescope Efficiency

T_π MeV central energy	ΔT_π MeV energy bite	ε_d non decay	ε_a non absorption	ε_s nuclear scattering	ε_m multiple scattering	$\varepsilon_d \cdot \varepsilon_a \cdot \varepsilon_m \cdot \varepsilon_s \cdot \varepsilon_\pi$ [a] net efficiency
20.9	3.54	0.517	0.993	0.999	0.794	.159
30.4	2.73	0.588	0.982	0.997	0.906	.203
52.3	2.27	0.670	0.932	0.991	0.885	.214
75.8	1.89	0.716	0.846	0.981	0.898	.208
99.9	1.71	0.745	0.745	0.967	0.893	.187

a Pion detection efficiency, ε_π, is 0.39.

TABLE IV

EXPERIMENTAL UNCERTAINTIES

Parameter		Percent
Contributions to Relative Accuracy:		
N_π	events, corrected for background	2 to 15
Ω	solid angle	1 to 3
ΔT_π	energy bite	1
ε_m	multiple scattering	0.3 to 1.7
ε_a	nuclear absorption	0.1 to 3.1
ε_s	nuclear scattering	0.1 to 1.8
ε_d	decay	< 0.5
N_t	target thickness	< 0.5
θ	production angle	1
Contributions to Normalization Accuracy		
N_p	number of incident protons	5
ε_{π^+}	π^+ detection factor	2.5
ε_{π^-}	π^- detection factor	10

PION PRODUCTION CROSS SECTIONS FOR BERYLLIUM in $\mu b \cdot MeV^{-1} \cdot sr^{-1}$

T_π (MeV)	Angle (deg) 60	90	120	135	150
π^+					
21	5.05 ± 0.24	6.21 ± 0.25	10.6 ± 0.04	8.83 ± 0.42	8.25 ± 0.52
30	5.35 ± 0.22	7.46 ± 0.33	11.7 ± 0.05	8.76 ± 0.36	8.77 ± 0.37
52	8.23 ± 0.28	7.68 ± 0.36	9.41 ± 0.36	6.75 ± 0.29	4.81 ± 0.16
76	8.29 ± 0.48	5.45 ± 0.30	4.77 ± 0.30	3.01 ± 0.17	
100	7.07 ± 0.47	2.95 ± 0.23	1.96 ± 0.16	0.97 ± 0.08	
π^-					
22	1.40 ± 0.25	1.48 ± 0.08	1.99 ± 0.11	2.17 ± 0.15	
32	1.86 ± 0.21	1.90 ± 0.17	2.32 ± 0.12	2.09 ± 0.12	
53	1.29 ± 0.14	1.36 ± 0.12	1.10 ± 0.07	1.32 ± 0.07	
76	0.94 ± 0.16	0.90 ± 0.10	0.28 ± 0.04	0.42 ± 0.03	
102		0.50 ± 0.06	0.07 ± 0.02		

TABLE VI

PION PRODUCTION CROSS SECTIONS FOR CARBON in $\mu b \cdot MeV^{-1} \cdot sr^{-1}$

T_π (MeV)	Angle (deg) 22	60	90	120	135	150
π^+						
21		8.17±0.36	10.1 ±0.5	13.7 ±0.5	12.2 ±0.5	14.1 ±0.7
30		9.41±0.4	11.4 ±0.4	15.8 ±1.0	12.9 ±0.6	13.8 ±0.6
52	9.30±0.38	11.3 ±0.5	11.3 ±0.4	13.1 ±0.6	9.70±0.36	8.87±0.25
76	16.8 ±0.9	10.3 ±0.6	9.07±0.58	7.35±0.50	5.39±0.28	
100	21.0 ±1.6	10.7 ±0.8	4.28±0.40	3.97±0.35	1.83±0.14	
π^-						
22		1.45±0.25	2.60±0.14	2.02±0.15	2.20±0.15	
32		2.72±0.36	3.65±0.05	3.29±0.16	2.70±0.14	
53		2.10±0.26	1.78±0.11	1.81±0.10	1.88±0.13	
76		1.41±0.15		0.60±0.05	0.63±0.05	
102			0.80±0.08	0.13±0.03		

TABLE VII

PION PRODUCTION CROSS SECTIONS FOR COPPER in $\mu b \cdot MeV^{-1} \cdot sr^{-1}$

T_π (MeV)	Angle (deg) 60	90	120	135	150
π^+					
21	18.4 ± 0.9	21.6 ± 1.1	32.7 ± 1.5	27.0 ± 1.5	22.2 ± 1.5
30	27.3 ± 1.1	27.8 ± 1.0	40.9 ± 1.7	32.3 ± 1.3	28.6 ± 1.4
52	27.2 ± 1.4	26.2 ± 1.3	34.3 ± 1.3	26.0 ± 1.2	
76	18.9 ± 1.3	20.8 ± 1.1	17.1 ± 0.9	12.9 ± 0.7	
100	12.1 ± 1.2	8.97± 0.71	6.75± 0.92	5.17± 0.43	
π^-					
22	8.3 ± 1.3	9.28± 0.50	8.97± 0.47	9.89± 0.69	
32	9.29± 0.81	9.73± 0.70	12.1 ± 0.7	9.03± 0.64	
53	4.66± 0.45	7.91± 0.43	4.42± 0.30	5.48± 0.37	
76	2.56± 0.44	4.85± 0.41	1.66± 0.13	1.33± 0.13	
102		2.57± 0.28	0.23± 0.09		

TABLE VIII

PION PRODUCTION CROSS SECTIONS FOR LEAD in $\mu b \cdot MeV^{-1} \cdot sr^{-1}$

T_π (MeV)	Angle (deg) 60	90	120	135	150
π^+					
21	26.4 ± 2.2	35.8 ± 2.2	42.9 ± 2.7	33.6 ± 2.3	29.9 ± 3.1
30	32.3 ± 2.1	46.4 ± 2.8	58.6 ± 3.9	51.1 ± 2.5	45.6 ± 3.5
52	28.2 ± 1.6	35.6 ± 1.9	49.3 ± 2.0	45.8 ± 2.5	39.3 ± 1.7
76	18.6 ± 1.2	21.5 ± 1.1	24.0 ± 2.7	22.7 ± 1.3	
100	12.9 ± 1.3	11.4 ± 1.4	9.2 ± 1.4	8.0 ± 1.2	
π^-					
22	29.9 ± 4.6	34.5 ± 2.7	30.8 ± 1.7	30.5 ± 2.0	
32	29.9 ± 3.4	34.3 ± 1.7	25.3 ± 1.7	23.0 ± 1.4	
53	18.2 ± 2.2	17.4 ± 1.3	12.2 ± 1.1	10.4 ± 0.7	
76	8.6 ± 1.2	5.8 ± 1.4	5.06± 0.47	4.74± 0.38	
102	4.3 ± 1.2		1.43± 0.15		

TABLE IX

TOTAL CROSS SECTIONS FOR π^+ AND π^- PRODUCTION BY 580 MeV PROTONS

Nucleus	σ_T^+ (mb)	σ_T^- (mb)	σ_T^+/σ_T^-
Be	17 ± 2	2.7 ± 0.3	6.3
C	20 ± 2	3.4 ± 0.4	5.9
Cu	35 ± 4	11 ± 1	3.2
Pb	50 ± 5	25 ± 3	2.0

FIGURE CAPTIONS

Figure 1 Experimental Arrangement

Figure 2 π^- and μ^- star detection factors ϵ_{π^-} and ϵ_{μ^-} as a function of the counter 4 discriminator level

Figure 3 Total reaction cross section curves for pion absorption by Cu and C used in the calculation of the nonabsorption factor ϵ_a. o reference 23, ● reference 20, ∀ reference 18, x reference 19, Δ reference 21, □ reference 22.

Figure 4 $d^2\sigma/dT_\pi d\Omega$ from carbon for positive pions at approximately 20° as a function of pion energy for various proton bombarding energies. Δ 21.5°, 450 MeV reference 5; o 21.5°, 595 MeV, reference 2; ∀ 19.5°, 660 MeV, reference 3; ● 20°, 730 MeV, reference 1; and □ 22°, 580 MeV, results reported here. Lines drawn through the data points are to guide the eye.

Figure 5 Comparison of $d^2\sigma/dT_\pi d\Omega$ for π^+ from carbon as a function of pion energy for result reported here at 580 MeV (——), and for 730 MeV (----) (reference 1) for various production angles. Lines drawn through the data points are to guide the eye.

Figure 6 Comparison of $d^2\sigma/dT_\pi d\Omega$ for π^- from carbon as a function of pion energy for results reported here at 580 MeV (——) and for 730 MeV (----) (reference 1) for various production angles. Lines drawn through the data points are to guide the eye.

Figure 7 Comparison of $d^2\sigma/dT_\pi d\Omega$ for π^+ for 580 MeV protons calculated by Beder and Bendix[6,7] for targets of C (——) and Cu (----) and the measured cross sections reported here for C (●) and Cu (x). The error bars on the measured points do not include the 6% normalization error. For the 22° production angle the data of Hirt *et al.* (o) is also plotted.

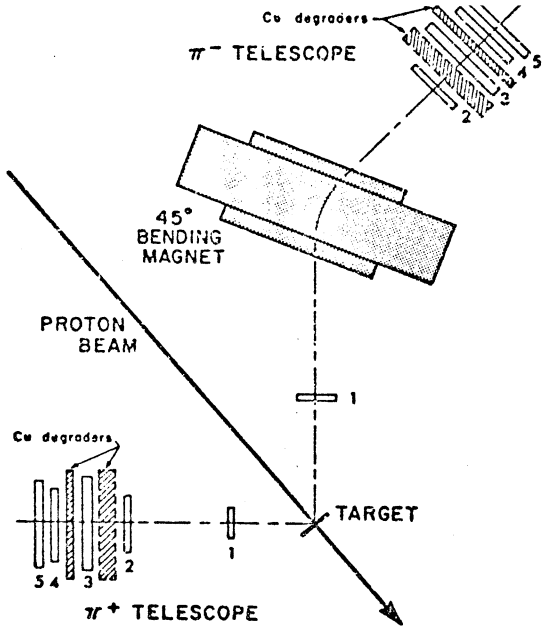

Fig. 1

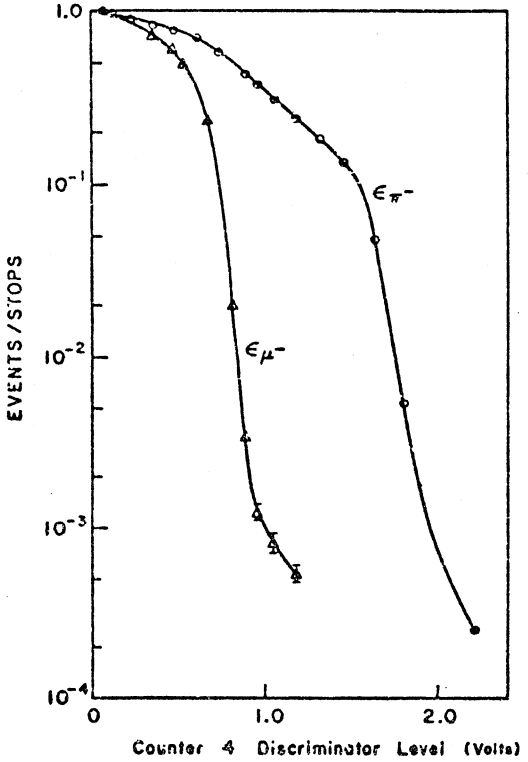

Fig. 2

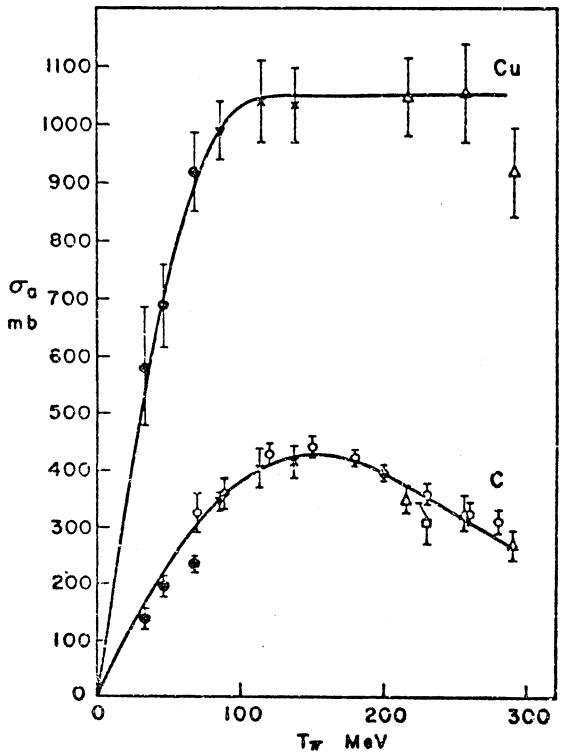

Fig. 3

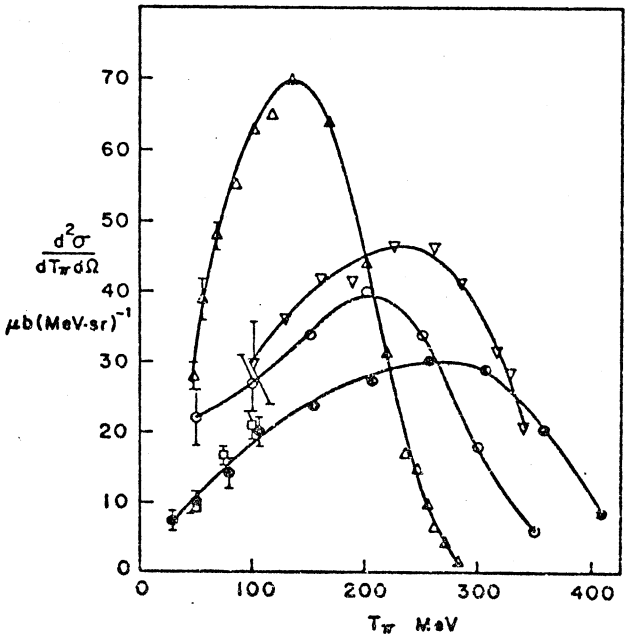

Fig. 4

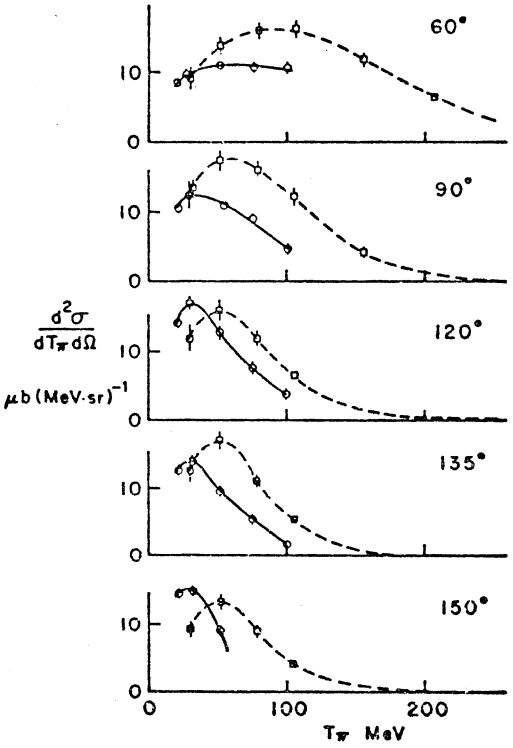

Fig. 5

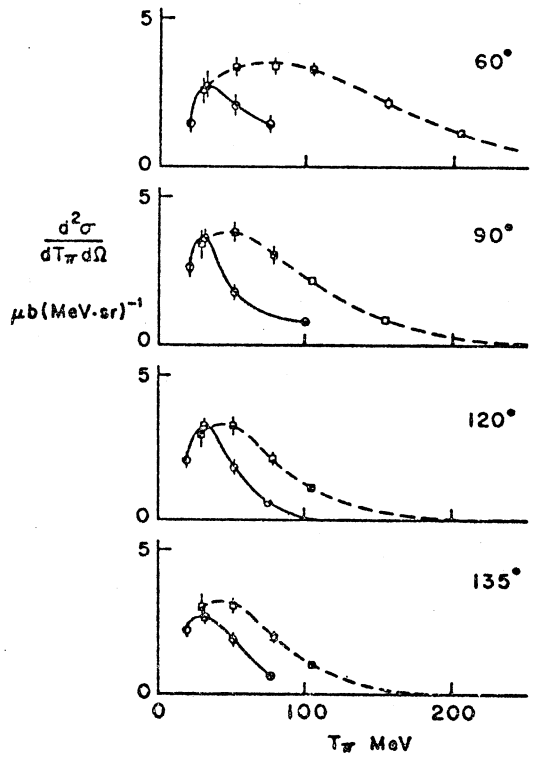

Fig. 6

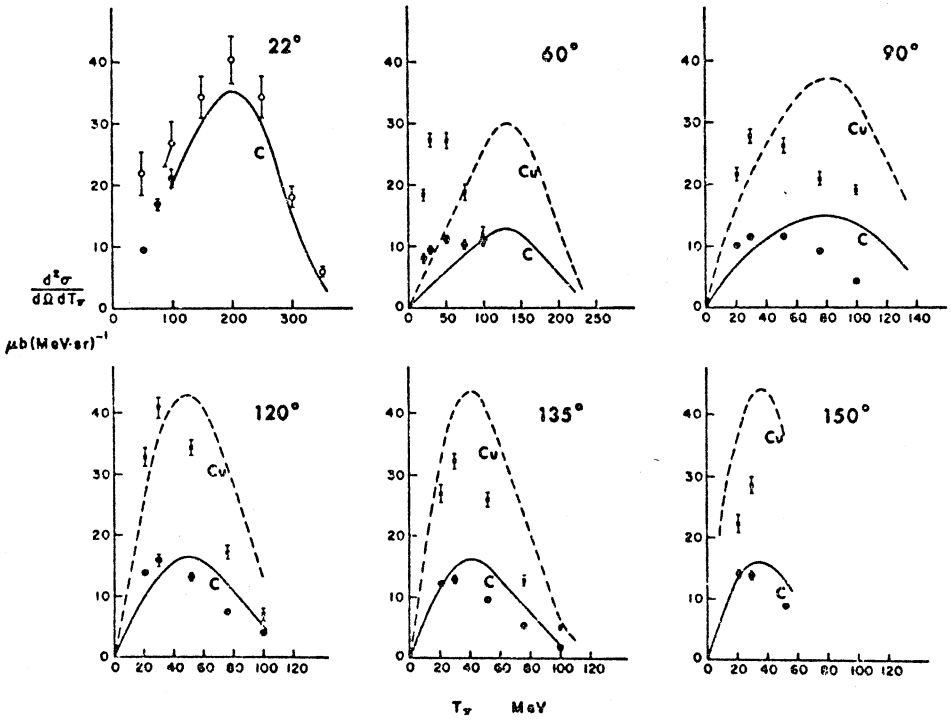

Fig. 7